8-2012

Atomistic simulations on multilayer graphene reinforced epoxy composites

Chunyu Li
Purdue University, Birck Nanotechnology Center, lichunyu@purdue.edu

Andrea R. Browning
Boeing Co

Stephen Christensen
Boeing Co

Alejandro Strachan
Purdue University, Birck Nanotechnology Center, strachan@purdue.edu

Li, Chunyu; Browning, Andrea R.; Christensen, Stephen; and Strachan, Alejandro, "Atomistic simulations on multilayer graphene reinforced epoxy composites" (2012). *Birck and NCN Publications.* Paper 879.
http://dx.doi.org/10.1016/j.compositesa.2012.02.015

Composites: Part A 43 (2012) 1293–1300

Contents lists available at SciVerse ScienceDirect

Composites: Part A

journal homepage: www.elsevier.com/locate/compositesa

Atomistic simulations on multilayer graphene reinforced epoxy composites

Chunyu Li [a], Andrea R. Browning [b], Stephen Christensen [b], Alejandro Strachan [a,*]

[a] School of Materials Engineering and Birck Nanotechnology Center, Purdue University, West Lafayette, IN 47906, United States
[b] Boeing Company, Seattle, WA 98124, United States

ARTICLE INFO

Article history:
Received 28 September 2011
Received in revised form 22 February 2012
Accepted 25 February 2012
Available online 6 March 2012

Keywords:
A. Carbon fibre
A. Polymer matrix composites (PMCs)
B. Interface/interphase
C. Computational modelling

ABSTRACT

We use molecular dynamics simulations to characterize multilayer graphene reinforced epoxy composites. We focus on two configurations, one where the graphene layers are parallel to polymer/graphene interface and a perpendicular case, and characterize the in situ curing process of the resin and the thermo-mechanical response of the composites. The yield stress of the composites under uniaxial loading normal to the interface is in all cases larger than that of the bulk polymer even after the constraint of the reinforcement to transverse relaxation is taken into account. While both the parallel and normal configurations have very similar strengths, the parallel case exhibits cohesive yield with strain localization and nano-void formation within the bulk polymer while the case with graphene sheets oriented normal to the interface exhibit interfacial debonding. These two mechanisms lead to different post yield behavior and provide key insight for the development of predictive models of carbon fiber polymer composites.

1. Introduction

Carbon fiber composites have applications in numerous industrial fields, especially in aircraft and aerospace industries. Understanding how the carbon fiber interacts with the polymer matrix at the atomistic level is important for evaluating the role of matrix adhesion to the overall composite performance. Carbon fibers are composed of graphite crystallites that are nanometers in size with the graphene sheets preferentially aligned along the fiber axis [1]. For polyacrylonitrile (PAN) based fibers of intermediate modulus (~280 GPa), the thickness in the stacking direction has been measured by X-ray diffraction (XRD) to be 3.5–6 nm [2,3], which is on the order of 10–20 graphene layers. XRD and Raman experiments have also shown a skin/core architecture for PAN fibers [3,4]. The radial architecture for PAN fibers has been determined using XRD to be a random orientation of crystallites [4,5]. Given the random nature of the crystallites orientation, the fiber surface consists of graphene edges with a distribution of angles relative to the radial direction.

Molecular simulations of the interaction of polyester and graphite have found strong adhesion when graphene is aligned parallel to interface [6,7]. The molecular structure of the interface between a polymer and graphite has also been characterized by atomistic simulations. A 10 Å thick interfacial region with bulk structure elsewhere was found by Mansfield and Theodorou [8] and density oscillations in the polymer matrix as a function of distance from the interfaces were found by Daoulas et al. [9]. More recently, the load transfer at the interface between polyethylene (PE) and a graphene sheet was studied by using molecular dynamics simulations [10]. Both normal tension and sliding shear were investigated with the result that separation occurred inside the polymer phase with a few PE chains maintaining adhesion to the graphene. This suggests that the intermolecular interactions between graphene and PE chains are stronger than those among the PE chains.

However, studies of the interaction between crosslinked epoxy-based thermosets and carbon fibers are scarce. We therefore report our atomistic simulations on multilayer graphene (MLG) reinforced epoxy composites. Two epoxy/amine formulations are considered: Diglycidyl ether of bisphenol A (DGEBA) known commercially as Epon 825 with 3,3′ Diamino-Diphenyl Sulfone (33DDS) and Diglycidyl ether of bisphenol C (DGEBC) also with 33DDS curing agent. We characterize the mechanical response of the resulting samples via non-equilibrium molecular dynamics (MD) simulations focusing on yield stress and post yield behavior. The resulting properties are compared to bulk resin simulations and similar simulations with pre-cured resin interacting with MLG [11].

2. Graphene/epoxy composite systems and simulation details

2.1. Simulations with DGEBA/33DDS

We simulate the curing processes of polymer matrix in the presence of MLG reinforcement using the procedure developed in Ref. [12]. The first step is to build an equilibrated mixture of the epoxy and curing agent molecules sandwiched between MLG of

* Corresponding author. Tel.: +1 765 496 6432.
E-mail address: Strachan@purdue.edu (A. Strachan).

1359-835X/$ - see front matter © 2012 Elsevier Ltd. All rights reserved.
doi:10.1016/j.compositesa.2012.02.015

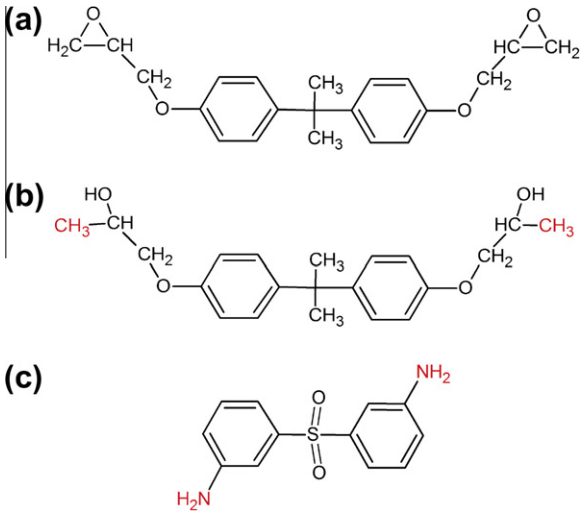

Fig. 1. Molecular structures of (a) DGEBA, (b) activated DGEBA, and (c) 33DDS.

interest. The model system of DGEBA and 33DDS is expressed as (n, m) with n being the number of epoxy molecules and m the number of curing agent molecules. We start with the "activated" DGEBA (as shown in Fig. 1) and place a small system of 16 epoxies and 8 amines (16, 8) in a periodic cell using software MAPS [13]. After a brief equilibration the simulation cell is replicated four times in each direction leading to a system of (1024, 512) with 69,120 atoms. The ratio of amine/epoxy is 1:2 for perfect stoichiometry, thus, in principle a 100% conversion could be reached.

Multilayer graphenes consist of layers of graphene bound together via van der Waals interactions. We chose multilayer graphene slabs with planes oriented parallel, Fig. 2a, and normal, Fig. 2b, to the polymer interface. The layers simulate the composite fiber reinforcement and characterize the two extreme configurations that can occur in carbon fiber reinforced composites. For the parallel MLG case, a six-layer graphene MLG is used. In normal MLG configuration the graphene layers are oriented with their in-plane direction normal to the interfaces and with thickness similar to that of the six-layer graphene. The MLGs were generated using a carbon bond length 1.418 Å with interlayer spacing 3.447 Å, considering the periodic boundary conditions and the estimated size of initial polymer slab. They were then equilibrated using an isothermal, isobaric (NPT) MD simulation at one atmospheric pressure for 10 ps using the Dreiding force field [14]. The final dimensions are 93.33 Å × 93.588 Å × 20.088 Å for parallel MLG and 93.588 Å × 93.744 Å × 19.648 Å. We assume partial atomic charges to be zero for graphene.

Before the polymerization simulations, the MLG samples and the DGEBA/33DDS mixture are combined into a single simulation cell. The (1024, 512) bulk system described above is equilibrated at 600 K and are transformed into a slab by extending the simulation cell length along the z direction to create a vacuum layer and their simulation cell parameters are adjusted to match those of the MLG along the two directions contained by the interface. The initial configurations of the layered cell are subsequently equilibrated with constant stress, isothermal MD simulations at 600 K and under atmospheric pressure. A Rahman–Parrinello barostat is used to obtain equilibrium simulation cell parameters for the composites, see Fig. 2 for a snapshot of the system.

All MD simulations of the DGEBA/33DDS system are carried out using LAMMPS, an open source MD code from US Sandia National Laboratories [15]. The general Dreiding force field [14] with harmonic form of potentials is employed in all simulations. For the van der Waals interactions we use, as in prior work [12], the Lennard–Jones 6–12 (LJ) potential during the crosslinking process and Buckingham (X6: exponential repulsion and power 6 attraction) during the annealing and testing process. Partial charges on DGEBA/33DDS are obtained from self-consistent calculations using the electronegativity equalization method as described in Ref. [12]. The accuracy of this in situ crosslinking method with the Dreiding force field and environment-dependence has been established in prior publications [12,16], in terms of elastic constants, glass transition temperature, and trends in the yield and post-yield behavior.

2.2. Simulations with resin represented as dendrimer

As described above, we compare the results for DGEBA/33DDS using a MD-based crosslinking procedure with those of DGEBC and 33DDS build using a dendrimer-based approach to create the model resin structure [17]. This dendrimer-based approach with the COMPASS force field has been extensively validated [18,19]. The dendrimer was constructed by successively connecting amine and epoxy monomers to create a highly branched molecule. The dendrimer used in the simulations was constructed using DGEBC monomers and 33DDS amine monomers, the final structure contains 6278 atoms and had an amine/epoxy ratio of 2/3.

The COMPASS force field [20] including partial charges and group-based cut-offs [21] for non-bonded interactions was used in the cell construction and subsequent simulations. After creation,

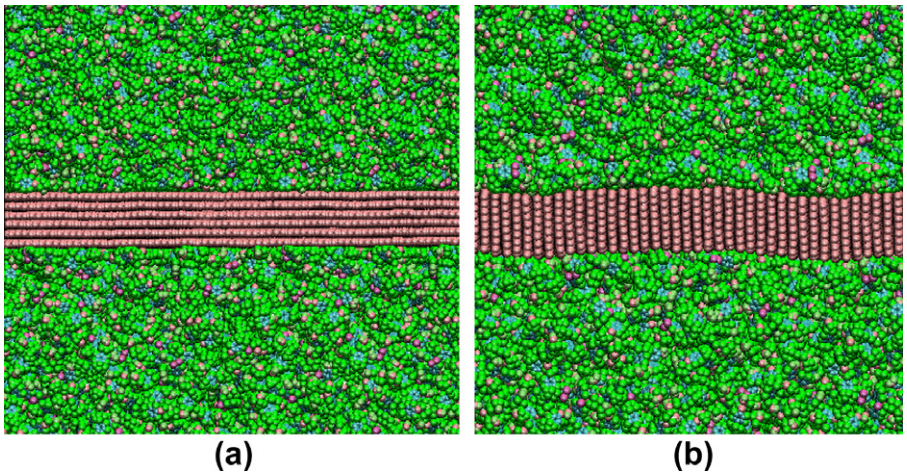

Fig. 2. DGEBA/33DDS with (a) a parallel MLG, and (b) a normal MLG, after 400 ps NPT equilibration.

the cell containing the dendrimer was annealed and compacted by a series of NVT and NPT molecular dynamics simulations beginning at 650 K and ending at 300 K. The Discover module of Materials Studio [22] was used for all the annealing and subsequent simulations. A final 250 ps NPT MD simulation at 300 K and atmospheric pressure was performed to equilibrate the cell (final density 1.147 g/cm^3).

The equilibrated dendrimer cell was layered with slabs of MLG, one slab with graphene sheets parallel to the interface and two slabs with sheets normal. The MLG slabs were constructed by replicating a graphite unit cell to dimensions that are approximately equal to the dendrimer cell. The graphene slabs are aligned so the direction normal to the interface was parallel to the *z* direction and dimensions of the dendrimer cell in the *x* and *y* directions were adjusted to match the MLG slab and the cell was re-equilibrated.

3. In situ polymerization of DGEBA/33DDS

We use a recently developed procedure to simulate the curing of thermoset polymers based on MD simulations where chemical reactions are performed in a stepwise manner using a distance-based criterion [12,16]. The details of our crosslinking procedure are described in Ref. [12] and only the key elements are presented here. Bonds are created between reactive atoms within a cutoff distance (5.64 Å, four times the equilibrium N–C bond length). New bonds are turned on slowly using a 50 ps long multi-step relaxation procedure to avoid large atomic forces. After the new bonds are fully relaxed an NPT simulation for an additional 50 ps is performed before a new set of bond creations is attempted. The curing process is simulated at a temperature of 600 K, well above the anticipated T_g of the cross-linked polymer (~500 K). This temperature is higher than typical actual curing temperatures of approximately 450 K. The high temperature in the simulations is desirable to increase molecular mobility and produce well-relaxed crosslinked structures [12]. The time required to achieve 85%, the predefined conversion degree limit for the systems in this paper, in the nanoscale composites (with polymer thickness of approximately 10 nm) is about three times longer than that for a bulk polymer. The slowdown is due to molecules near the graphite interface having a lower coordination number and consequently a lower chance of chemically reacting, similar to the case of free-standing films [23]. The 85% conversion limit is chosen as a compromise between simulation time and achieving a realistic degree of cure [12]. Based on our experience, higher conversion is difficult to reach due to the relatively short timescales involved in MD simulations. This is particularly true for thin slabs where surface molecules are under-coordinated, see Ref. [21]. Experimentally, conversions in the 85–95% are common in bulk polymers and, as mentioned, slabs are expected to have lower conversion. During the process of crosslinking, the network is growing continuously while the volume decreases with increasing conversion degree. The shrinking percentages are about 8.6% for composite with parallel MLG and 9.9% for composites with normal MLG.

Due to the atomic nature of our simulations, molecular details of the chemical reactions during crosslinking can be tracked, with the objective of correlating the topology of the network and its response. Before crosslinking, the total number of reactive carbon atoms is twice the number of DGEBA monomers and the total number of nitrogen atoms with two reactive sites is also two times number of 33DDS monomers. To determine the distributions of these reactive sites we divide the slab into 55 bins along its thickness and compute the number density of reactive atoms, carbons and nitrogens, which can belong to either the oxirane ring or a primary (denoted N_p below) or secondary (N_s) amine. The number density of reactive sites along the slab thickness before crosslinking shows the typical fluctuations expected in small systems but also a slight gradient in the distribution of primary amine N_p; the reactive carbon atoms are more evenly distributed. The origin of this small gradient is not clear at this point because the distributions of reactive sites at the initial slab just created from a bulk are more balanced. But after 400 ps equilibration a slight gradient appears and it may be a result of the stochastic nature of the simulations.

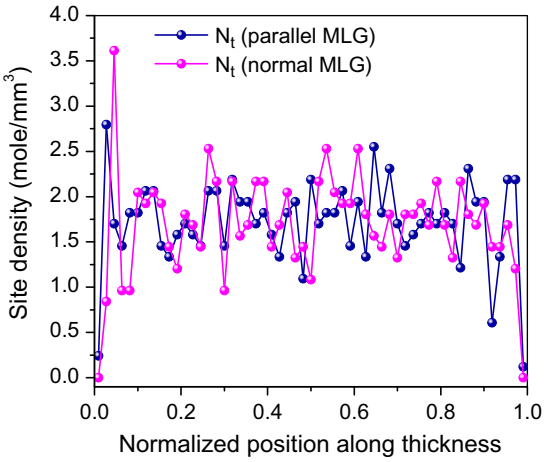

Fig. 3. Distribution of fully reacted sites.

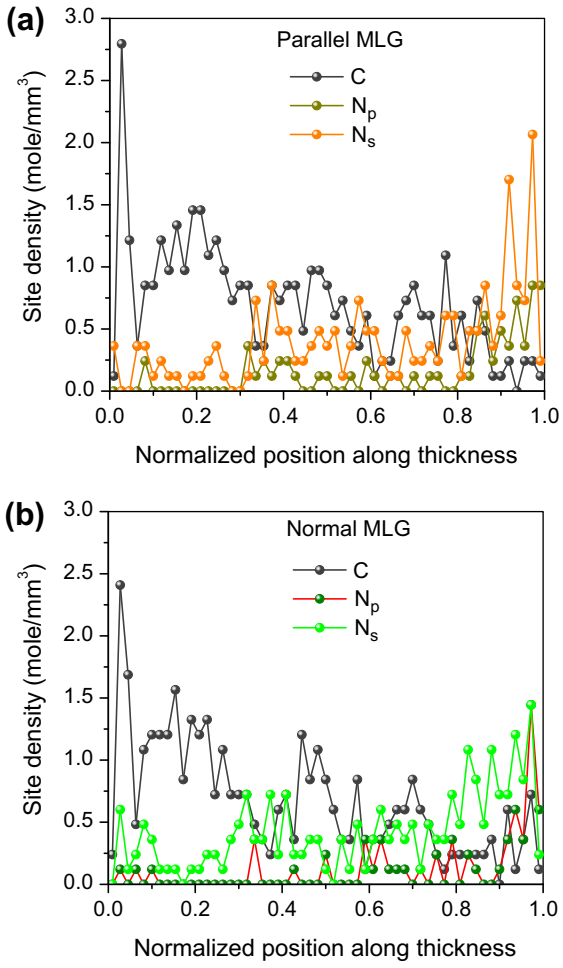

Fig. 4. Distribution of unreacted sites.

After crosslinking the system up to a conversion of 85%, we re-analyzed the number density of fully reacted nitrogen atoms (tertiary amine, denoted as N_t) (Fig. 3) and remaining reactive sites (Fig. 4). We find that for both normal and parallel composite systems the distributions of fully reacted nitrogen atoms is homogeneous in the slab thickness direction despite the initial unbalanced distributions of carbon and nitrogen atoms indicating that the crosslinked polymers have a uniform distribution of connecting sites through the thickness of the polymer slab. Interestingly, the distributions of unreacted atoms show spatial variations with unreacted carbon atoms concentrated near one interface of the slabs and unreacted N concentrated near the other. The unreacted C and primary amine N represent ends of polymer chains and are the potential locations for void nucleation due to the weaker nature of non-bond interactions compared with covalent bonding interactions at reacted sites.

4. Density profiles

As conversion proceeds, the average density of the polymer layer increases and the thickness of the polymer slab decreases. The cool-down of the model system to room temperature further increases the density. Fig. 5 shows the density profiles of polymer slab at different temperatures. It is seen that oscillations in the polymer density are near the graphite surface. The van der Waals interactions between the polymer atoms and those in the closely packed graphite surface cause these oscillations. Short-range repulsion leads to an exclusion region next to the surface followed by a density maximum as a first layer of polymer atoms packs against the surface due to attractive van der Waals interactions. This first layer of atoms leads to a second exclusion region and a local minimum in density followed by a second layer of atoms and density maximum. The effect of the graphene surface atoms diminishes away from the interfaces and the oscillations decay rapidly. This behavior is equivalent to what is observed in the radial distribution functions of simple liquids and amorphous solids. The thickness of the interfacial region is approximately 7 Å, or about twice the van der Waals radii, and rather insensitive to temperature, as highlighted in Fig. 5. These results are similar to the observations in Ref. [9] for a polyethylene melt adsorbed on graphite. The average of predicted density at 300 K for the polymer slab with 85% conversion is 1.17 ± 0.03 g/cm^3, which is in very good agreement with the experimental value of $\sim$1.23 g/cm^3 for DGEBA/DDS [24].

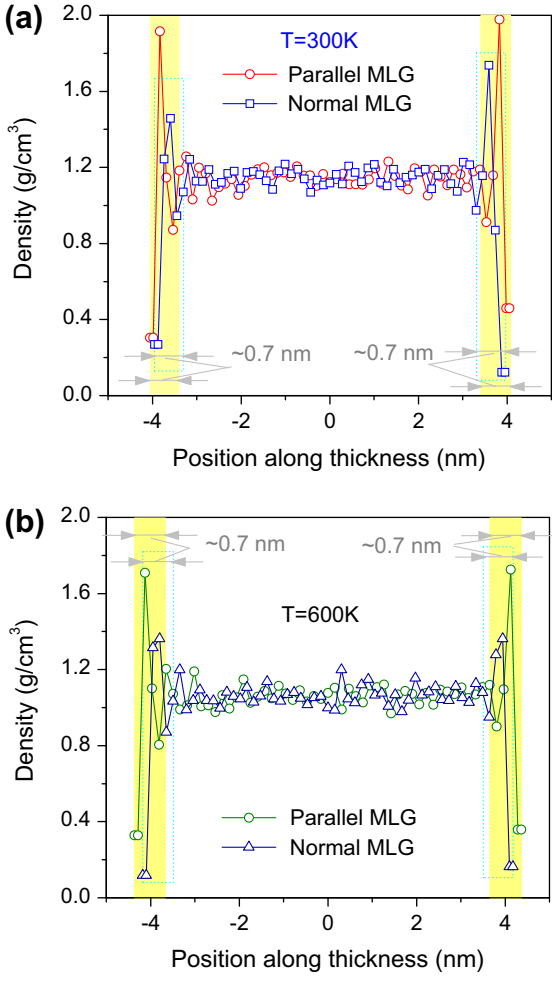

Fig. 5. Density profiles at different temperatures of 85% converted system.

5. Ultimate mechanical response of epoxy/MLG composites under uniaxial tension

The in-plane tensile strength of MLG is in the 100–130 GPa range [25] and its out-of-plane tensile strength between 1 and 5 GPa [26]. In contrast, polymers, either thermoplastics or thermosets, usually have tensile strengths in the tens to hundreds of megapascals. The elastic constants of the two components are also widely different which lead to stress concentrations and mechanical constraints in the composites that play key roles in their overall mechanical response. In this study, we focus on the tensile deformation of graphene/polymer composite in the direction normal to the interface. This is carried out via non-equilibrium MD simulations where the composites are deformed at a constant strain rate of 5×10^8 s^{-1} along the direction normal to the MLG/polymer interface while maintaining atmospheric pressure in other two transverse directions using a barostat. LAMMPS uses a Holian et al. [27] thermostat and Parrinello–Rahman [28] barostat. This mixed-boundary conditions method is similar to the $NTL_xS_{yy}S_{zz}$ ensemble method proposed by Yang et al. [29].

Fig. 6 shows the stress–strain curves for uniaxial tension in the direction normal to the polymer/MLG interface for both parallel and normal DGEBA/33DDS composites. For comparison, we show stress strain curves of the bulk polymer both for uniaxial stress conditions (atmospheric stress in the transverse directions) and for pure uniaxial strain (where no lateral relaxation is allowed). The yield stresses of both composites are very similar to that of

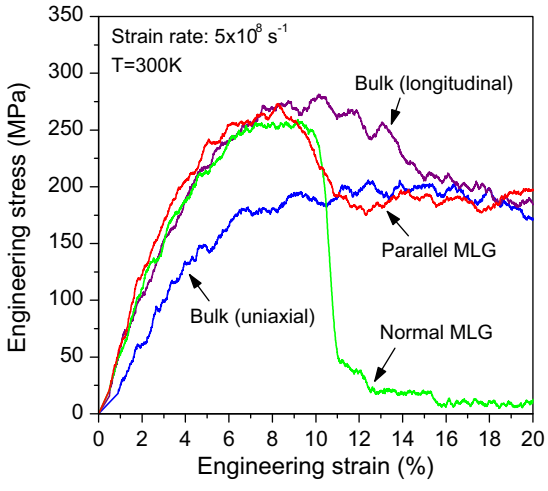

Fig. 6. Stress–strain relationship for tension in the direction normal to interface.

the bulk polymer with lateral constraint and over 30% larger than that of the unconstrained polymer. Fig. 6 clearly shows that the main role of the reinforcements is to provide constraints to the mechanical deformation of the polymer leading to significant strengthening of the polymer phase. While both parallel and normal MLG composites exhibit nominally identical strengths their post-yield behavior is very different, the normal MLG case looses all strength very abruptly after yield while the parallel MLG case retains strength in a manner similar to that of the bulk polymers.

To better understand the yield and post-yield processes in the composites we now analyze the molecular processes associated with the uniaxial deformation. Our simulations show strain localization in the bulk polymer for the parallel MLG case and interfacial debonding in the normal MLG. Fig. 7 shows snapshots of the parallel MLG composite under tension in the direction normal to the interface. To best observe the evolution of failure only partial systems are shown. The parallel case at 10% strain (right after yield) shows the presence of nanoscale voids in the bulk of polymer slab, located approximately 2.0 nm from the interface. With continuing deformation the voids grow and coalesce and at 15% strain a nanovoid approximately 1.0 nm in size is visible across the sample. The nanovoid continues to grow under tension while smaller voids at other locations become visible, see Fig. 7c. Interestingly, the thin MLG sections bends during yield due to a local gradient in strain caused by the damaged polymer. This occurs due to the low flexural stiffness of the MLG with only six layers; in contrast, the composites with dendrimer-built polymers and thicker MLG sections (12 graphene sheets) did not show bending.

For the normal MLG composite, yield and failure under tension occurs via a completely different process, despite the similar yield stress (Fig. 8). The composite fails due to interfacial debonding with all the damage concentrated at the interface. Note that the interface failure develops rather quickly and this localization is responsible for the abrupt loss of strength. At a strain of approximately 10%, nanovoids (diameter $\sim$1.0 nm) begin to form at the interface. At approximately 15% strain, the polymer slab and the MLG are almost completely separated.

The difference in these failure mechanisms can be attributed to the adhesion of polymer to the MLG. Although the van der Waals interaction between polymer and MLG atoms are identical in both cases, the larger atomic density in the parallel MLG case leads to a larger energy density and stronger interfacial adhesion. The interface of the normal MLG exhibit rows of C atoms separated by van der Waals distances. The implication of these results for carbon fiber composites is that debonding is likely initiated in regions of the fibers with graphene layers normal to the polymer interface.

Similar tension simulations were performed on the dendrimer/MLG cells described in Section 2.2. A strain rate of $5 \times 10^8\ s^{-1}$ (using 0.1% strain steps applied every 2 ps) was applied in the z direction while holding the other dimensions constant (a condition slightly different from the DGEBA/33DDS simulations in which lateral dimension is allowed to adjust to maintain atmospheric stress). For comparison, the bulk dendrimer polymer was also deformed. Longitudinal tension was applied to the bulk cell by straining in one direction and maintaining the simulation cell length the transverse directions constant. Uniaxial tension was applied to the bulk cell by straining in one direction and applying a Poisson's ratio of 0.33 to the other directions. For both the longitudinal and uniaxial tension simulations the strain rate was $5 \times 10^8\ s^{-1}$ and results are averaged over simulations applying the tension in the x, y, and z direction.

The stress perpendicular to the interface observed during the tension simulations for the normal and parallel MLG layered cells is shown in Fig. 9 as a function of engineering strain along with the results for the bulk polymer. The parallel MLG layered cell data shown is for the zigzag MLG, but similar results were observed

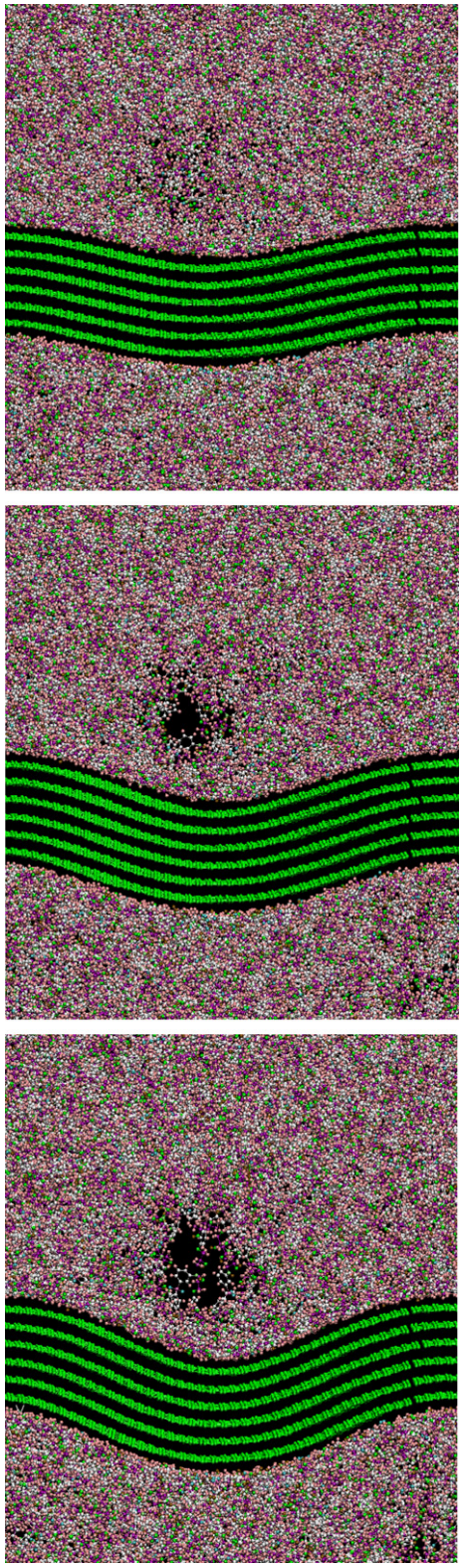

(a) 10% strain

(b) 15% strain

(c) 20% strain

Fig. 7. Polymer failure under uniaxial tension in the direction normal to the interface.

with the chair MLG. As observed in the DGEBA/33DDS case, the location of post yield strain localization as evidenced by void formation during the tension simulations varies between the parallel and the normal MLG layered cells. In the parallel MLG cell and voids appear in the resin. Fig. 10 shows the layered cell

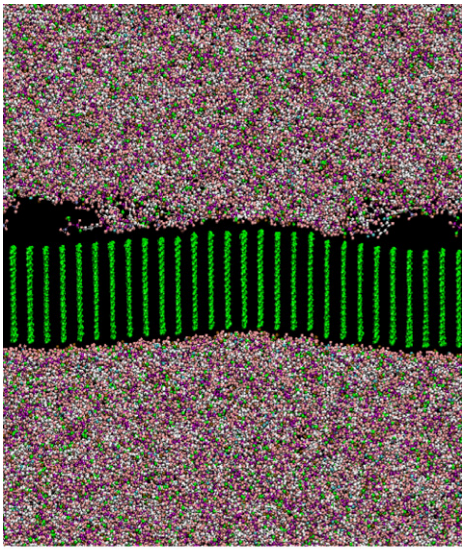

(a) 10% strain

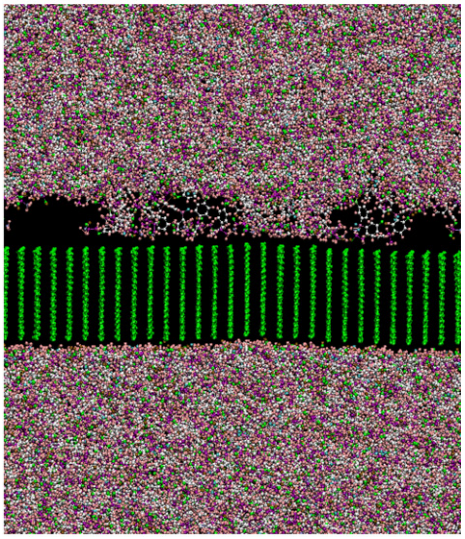

(b) 11% strain

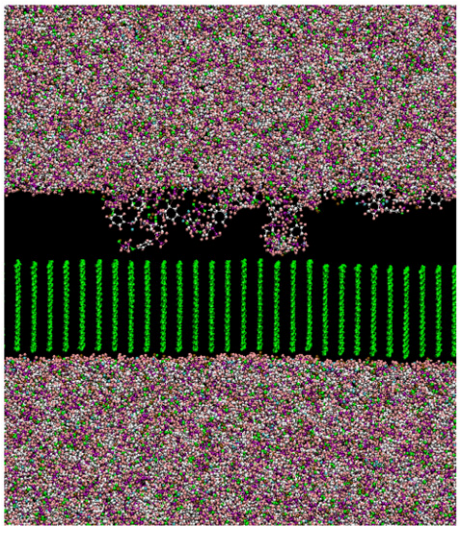

(c) 15% strain

Fig. 8. Interface failure under uniaxial tension in the direction normal to the interface.

configuration at various strain levels. Lower density regions can be seen in the resin at ~8% strain, corresponding to the post yield drop in the stress vs. strain plot (see Fig. 9). After the softening,

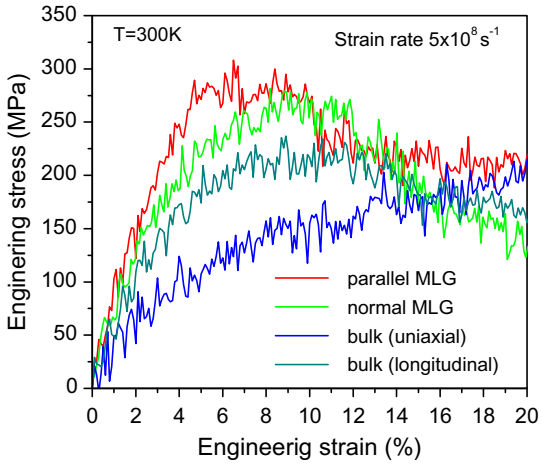

Fig. 9. Stress–strain relationship for tension in the direction normal to graphene.

the curve follows the uniaxial bulk stress vs. strain curve. At 13% strain a void of ~1 nm can be seen percolating through the resin. The same void grows larger as more strain is applied, but the interaction between the resin and graphite is maintained as can be seen in the 17% strain image. The normal MLG layered cell exhibits interfacial debonding rather than void formation in the resin in agreement with the DGEBA/33DDS results. The debonding of the interface from 8% strain to 17% strain can be seen in Fig. 11. A drop in stress is observed at the same strain level as debonding (see Fig. 9) and the normal MLG system loses strength faster than the cases where strain localization occurs in the bulk polymer, this is also in qualitative agreement with the DGEBA/33DDS results.

6. Discussion

An analysis of the dendrimer-built DGEBC/33DDS and the in situ cured DGEBA/DDS composites provide important insight into epoxy interactions with graphene and the role of reinforcements in the composite performance. Our results show that the interfacial adhesion between the epoxies and MLG is sufficient for the strength of the composites under uniaxial tension to be larger than that of the bulk polymer. This is true even after mechanical constraints are taken into account: in all cases as seen in Figs. 6 and 9, the strength of the composites is larger than that of the bulk polymer even when transverse relaxation is not allowed. Furthermore, for both types of resins, normal MLG composites exhibit interfacial debonding while parallel MLG shows strain localization in the bulk polymer. This supports the conclusion that the adhesion of the polymer epoxies to the MLG (interacting only by van der Waals forces) is strongly influenced by the orientation of the MLG with respect to the interface due to its influence on the density of carbon atoms at the interface. This effect can be quantified by the interfacial energy $U_{interface}$ defined as:

$$U_{interface} = (PE_{resin} + PE_{MLG} - PE_{composite})/A \quad (1)$$

where $PE_{composite}$ is the total potential energy of the composite cell, PE_{resin}, PE_{MLG} are the potential energies of the isolated resin slab and MLG and A is the interface area. A large vacuum space was added to an equilibrated cell so that there was only one interface in a model cell. The results of the interfacial energy calculations are DGEBA/33DDS: 0.29 (parallel MLG), 0.17 (normal MLG); Dendrimer: 0.37 (parallel MLG), 0.21 (normal MLG). A positive value of interfacial energy indicates that bringing the resin and MLG together is energetically favorable. The parallel MLG configuration has an interfacial energy almost twice as large as the normal MLG; this can be

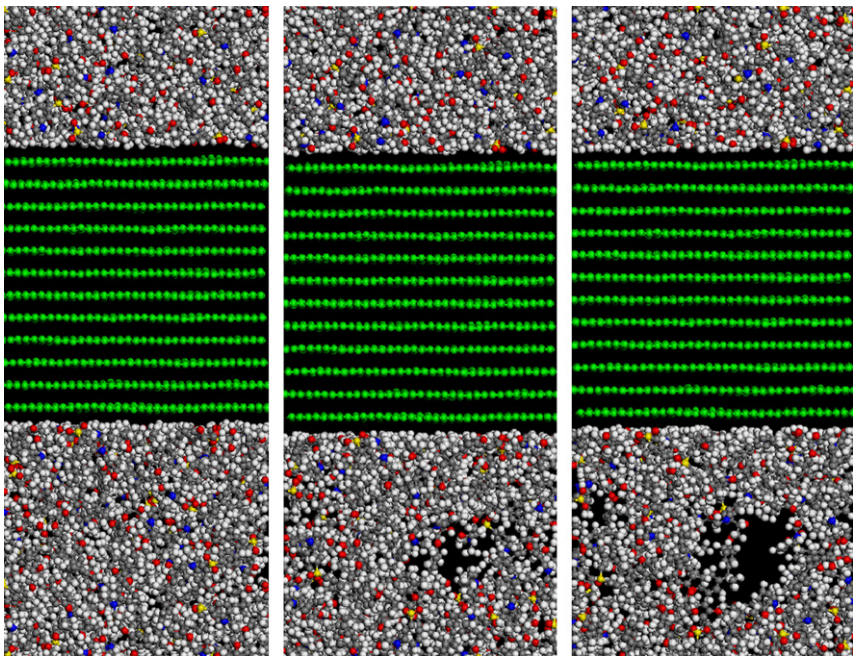

(a) 8% strain (b) 13% strain (c) 17% strain

Fig. 10. Dendrimer system shows polymer failure under uniaxial tension in the direction normal to the interface.

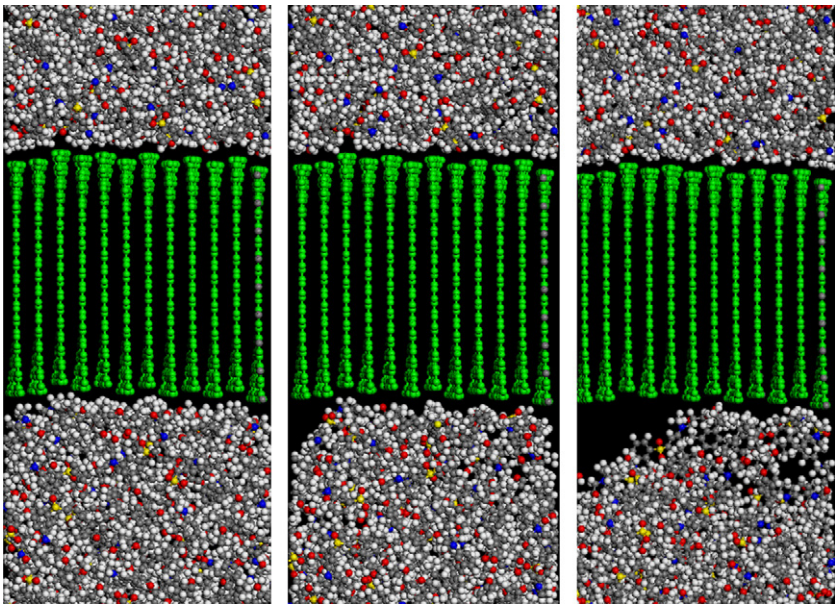

(a) 8% strain (b) 13% strain (c) 17% strain

Fig. 11. Dendrimer system shows interface failure under uniaxial tension in the direction normal to the interface.

compared with the number density of atoms on the graphene surface ~38 atoms/nm^2 for parallel MLG and ~14 atoms/nm^2 for normal MLG. Though the interfacial energy does not always correlate with failure location [30], the difference in interface energy explains the location of void formation behavior of the two types of composites investigated here. The results presented in this paper are also supported by experimental observation of both adhesive and cohesive failures in carbon fiber/epoxy composites [31,32]. It is important to note that the strain rate in our MD simulations (10^8 s^{-1}) is several orders of magnitude higher than that used in experiments. Such fast deformation rates lead to an overestimation of the yield stress; however, despite such limitation, MD simulations capture non-trivial trends in yield and post yield behavior of amorphous polymers including the role of thermal history, temperature and loading path; see for example Refs. [16,33]

While there are differences between the stress–strain curves of the two models, in both cases we observe very similar trends: (i) The strength of the composites in tension (regardless of graphite orientation) is very similar to that of the neat resins under pure uniaxial strain (no lateral relaxation) conditions. This shows the role of the carbon reinforcements and that van der Waals interactions are enough to produce high-quality interfaces. (ii) In

the case of graphene layers parallel to the interface yield and post-yield deformation are dominated by bulk polymer processes. (iii) When the graphene layers are perpendicular to the interface we observe interfacial decohesion. Several factors can contribute to the differences in stress–strain curves observed between the two models. First, system size differences; the MLG volume fraction in the dendrimer-based composite is approximately 50% and only 20% in the in-site built polymer model. Higher MLG volume results in the dendrimer-based polymer experiencing a larger strain rate than the in situ cured system resulting in higher yield and flow stress; this is consistent with the results of Figs. 6 and 9.

As in all prior MD simulations of polymers and other materials the predicted strains are large compared to macroscopic experiments; see [33] and references therein. Such large strains are attributed to the small size of the MD simulation cells that preclude strain localization [16,33]. This is consistent with recent nano-indentation experiments in cross-linked polymers that reported strains of approximately 25% [34] such deformation levels would not be achievable over larger scales. Thus, a direct comparison of MD results at the nanoscale and experiments at the macroscale should only be done in a qualitative manner.

7. Conclusions

We carried out atomistic simulations on the curing process and mechanical response of thermoset polymer composites reinforced with multilayer graphene. The graphene sheets were taken to be parallel with or normal to the interface. Compared with bulk polymers, the curing of the thin slabs of polymer between MLG is slowed down for conversion degrees over 70% due to surface effects. The interaction with atomistically sharp MLG interfaces leads to density oscillations in the polymer over a narrow ($\sim$0.7 nm) interfacial region. Regardless of the relative orientation of the MLG and the composite interface the strength of the composites under uniaxial tension are higher than the corresponding value for the bulk polymer. However, the parallel MLG exhibits a stronger interface (higher interfacial energy) leading to cohesive failure in the bulk polymer. On the contrary, the normal MLG case exhibits adhesive failure at the interface leading to a more brittle behavior and steeper post yield softening due to its ability to localize deformation at the interface. These results are critical to understand the performance of composites based on carbon fibers whose complex nanostructure leads to a variety of orientations of the graphene crystals on the surface.

Acknowledgments

This work was supported by a grant with The Boeing Company and the US National Science Foundation (NSF) under contract CMMI-0826356. Useful discussions with R.B. Pipes and J. Gosse are gratefully acknowledged.

References

[1] Liu FJ, Wang HJ, Xue LB, Fan LD, Zhu ZP. Effect of microstructure on the mechanical properties of PAN-based carbon fibers during high-temperature graphitization. J Mater Sci 2008;43:4316–22.
[2] Loidl D, Paris O, Rennhofer H, Müller M, Peterlik H. Skin-core structure and bimodal Weibull distribution of the strength of carbon fibers. Carbon 2007;25(14):2801–5.
[3] Huang Y, Young RJ. Effect of fiber microstructure upon the modulus of pan-and pitch-based carbon-fibers. Carbon 1995;33(2):97–107.
[4] Paris O, Loidl D, Peterlik H. Texture of PAN- and pitch-based carbon fibers. Carbon 2002;40(4):551–5.
[5] Zhou GS, Liu YQ, He LL, Guo QG, Ye HQ. Microstructure difference between core and skin of T700 carbon fibers in heat-treated carbon/carbon composites. Carbon 2011;49:2883–92.
[6] Henry DJ, Lukey CH, Evans E, Yarovsky I. Theoretical study of adhesion between graphite, polyester and silica surfaces. Mol Simul 2005;31:449–55.
[7] Yiapanis G, Henry DJ, Evans E, Yarovsky I. Effect of aging on interfacial adhesion between polyester and carbon-based particles: a classical molecular dynamics study. J Phys Chem C 2007;111:6465–72.
[8] Mansfield KF, Theodorou DN. Atomistic simulation of a glassy polymer/graphite interface. Macromolecules 1991;24:4295–309.
[9] Daoulas KC, Harmandaris VA, Mavrantzas VG. Detailed atomistic simulation of a polymer melt/solid interface: structure, density, and conformation of a thin film of polyethylene melt adsorbed on graphite. Macromolecules 2005;38:5780–95.
[10] Awasthi AP, Lagoudas DC, Hammerand DC. Modeling of graphene–polymer interfacial mechanical behavior using molecular dynamics. Modell Simul Mater Sci Eng 2009;17:015002.
[11] Browning A. Utilization of molecular simulations in aerospace materials: simulation of thermoset resin/graphite interactions. Proc of AIChE annual meeting; 8–13 November 2009.
[12] Li CY, Strachan A. Molecular simulations of crosslinking process of thermosetting polymers. Polymer 2010;51(25):6058–70.
[13] MAPS-The Materials And Processes Simulations platform, Scienomics Inc. <http://www.scienomics.com>.
[14] Mayo SL, Olafson BD, Goddard III WA. Dreiding: a generic force field for molecular simulations. J Phys Chem 1990;94:8897–909.
[15] LAMMPS-Large-scale Atomic/Molecular Massively Parallel Simulator. <http://lammps.sandia.gov>.
[16] Li CY, Strachan A. Molecular dynamics predictions of thermal and mechanical properties of thermoset polymer EPON862/DETDA. Polymer 2011;52(13):2920–8.
[17] Christensen S. Atomistically explicit molecular dynamics simulations of thermosetting polymers. Proc of 39th ISTC SAMPE conf; 2007.
[18] Knox CK, Andzelm JW, Lenhart JL, Browning AR, Christensen S, High strain rate mechanical behavior of epoxy networks from molecular dynamics simulations. Proc of 27th army science conf, Orlando, FL, GP-09; December 2010.
[19] Rigby D, Sun H, Eichinger BE. Computer simulations of poly(ethylene oxides): forcefield, PVT diagram and cyclization behavior. Polym Int 1998;44:311–30.
[20] Sun HJ. COMPASS: an *ab initio* force-field optimized for condensed-phase applications-overview with details on alkane and benzene compounds. Phys Chem B 1998;102(38):7338–64.
[21] Leach AR. Molecular modeling: principles and applications. London: Longman; 1996.
[22] Materials Studio by Accelrys Software Inc. <http://accelrys.com>.
[23] Li CY, Strachan A. Effect of thickness on the thermo-mechanical response of free-standing thermoset nanofilms from molecular dynamics. Macromolecules 2011.
[24] Enns JB, Gillham JK. Effect of the extent of cure on the modulus, glass-transition, water-absorption, and density of an amine-cured epoxy. J Appl Polym Sci 1983;28:2831–46.
[25] Lee C, Wei XD, Kysar JW, Hone J. Measurement of the elastic properties and intrinsic strength of monolayer graphene. Science 2008;321(5887):385–8.
[26] Hupp TR. Graphite, properties of artificial. In: Kirk-Othmer encyclopedia of chemical technology. New York: John Wiley & Sons, Inc; 1992.
[27] Holian BL, Degroot AJ, Hoover WG, Hoover CG. Time-reversible equilibrium and nonequilibrium isothermal–isobaric simulations with centered-difference Stoermer algorithms. Phys Rev A 1990;41:4552–3.
[28] Parrinello M, Rahman A. Polymorphic transitions in single crystals: A new molecular dynamics method. J Appl Phys 1981;52:7182.
[29] Yang L, Srolovitz DJ, Yee AF. Extended ensemble molecular dynamics method for constant strain rate uniaxial deformation of polymer systems. J Chem Phys 1997;107:4396–407.
[30] Gersappe D, Robbins MO. Where do polymer adhesives fail? Europhys Lett 1999;48:150–5.
[31] Chou CT, Gaur U, Miller B. Evaluation of fracture surfaces in carbon fiber/epoxy composites. J Adhesion 1993;40:245–56.
[32] Koyanagi J, Yoneyama S, Eri K, Shah PD. Time dependency of carbon/epoxy interface strength. Compos Struct 2010;92:150–4.
[33] Jaramillo E, Wilson N, Christensen S, Gosse J, Strachan A. Energy-based yield criterion for PMMA from large-scale MD simulations. Phys Rev B 2012;85:024114.
[34] Altebaeumer T, Gotsmann B, Knoll A, Cherubini G, Duerig U. Self-similarity and finite-size effects in nano-indentation of highly cross-linked polymers. Nanotechnology 2008;19:475301.